Scientific
Research
Publishing

Contrast of Perspectives of Coherency

Tian Ma, Erik Bollt

Department of Mathematics and Computer Science, Clarkson University, Potsdam, NY, USA
Email: mat@clarkson.edu, bolltem@clarkson.edu

Abstract

Mixing and coherence are fundamental issues at the heart of understanding fluid dynamics and other non-autonomous dynamical systems. Recently the notion of coherence has come to a more rigorous footing, in particular, within the studies of finite-time nonautonomous dynamical systems. Here we recall "shape coherent sets" which is proven to correspond to slowly evolving curvature, for which tangency of finite time stable foliations (related to a "forward time" perspective) and finite time unstable foliations (related to a "backwards time" perspective) serve a central role. We compare and contrast this perspective to both the variational method of geodesics [17], as well as the coherent pairs perspective [12] from transfer operators.

1. Introduction

Understanding and describing mixing and transport in two-dimensional fluid flows have been a classic problem in dynamical systems for decades. Here we focus on three theories related to coherence in finite-time nonautonomous dynamical systems: 1) Shape coherent sets [22] where the nonlinear flow itself as considered to be special "shape coherent sets" reveals that the otherwise complicated flow reduces to a simpler transformation, namely rigid body transformations, on the corresponding time and spatial scales; 2) The geodesic theory of transport [17] which initially describes that transport barriers relate to minimally stretching material lines ("Seeking transport barriers as minimally stretching material lines, we obtain that such barriers must be shadowed by minimal geodesics under the Riemannian metric induced by the Cauchy-Green strain tensor." [17]) and later it was improved to "stationary values of the averaged strain and the averaged shear," [18]; 3) Coherent pairs [2] [12] [21] viewed by transfer operators in terms of evolving density. See **Table 1**. Not all methods are coverer here, notably the combination method of Tallapragada and Ross [26] which gives FTLE like quantities directly from transfer operator.

In this paper, we contrast three perspectives of coherence by calculating several objective measures which are a) the evolution of arc length; b) the relative coherence pairing; c) foliation angles; d) change of curvature; e) registration of shapes; and f) the shape coherence factor for sets developed from each of these methods, two of which are respectively shown in **Tables 1-3**. We show that each of these three perspectives of coherence may keep its advantages on its corresponding measure. According to a geodesic perspective, arc length should vary

Table 1. Comparison assumptions between three theories of coherence.

Theory	Measures	Design	Related Keywords
Shape coherent sets	Shape coherence factor $\alpha(A,B,T)$	Preserving shape. Regularity link between curvature and shape coherence	Finite-time stable/unstable foliation, nonhyperbolic splitting angles, slow evolving curvature, FTC.
Geodesic transport barrier	Arc length evolution	Stationary values of the averaged strain and the averaged shear	Hyperbolic, elliptic and parabolic barriers Lagrangian coherent structures. [9] [16] [17]
Coherent pairs	Coherent pair number $\rho_\mu(A_t, A_{t+\tau})$	Minimizing density loss, Frobenius-Perron operator by Ulam-Galerkin's matrix, SVD	Coherent pairs, hierarchical partitions, Galerkin-Ulam matrices. [2] [12] [21]

Table 2. Comparison between three theories of figures of merit shown of evolution of the double gyre system. Compare to the geometry of the evolution of the sets discussed in **Figure 3** and illustration of these measures in **Figure 4**, and discussion in the caption. It can be seen that each performance on their own measure, but also quite well in the alternative measures. This partly reflects that similar sets can be found from each method, but not necessarily always.

Theory	$\alpha(A,B,T)$	Arc Length Change (%)	$\rho_\mu(A_t, A_{t+\tau})$	Specification
Shape coherent sets	0.9637	1.14%	1	The grid size is 200 by 200. See **Figure 3** left column.
Geodesic transport barrier	0.9362	0.93%	1	Calculated by LCStool [19]. See **Figure 3** right column.
Coherent pairs	0.9210	1.9%	0.995	50,000 by 50,000 matrix with 20 million sample points. See **Figure 4**.

Table 3. Comparison among three theories on the Rossby wave system. See **Figure 6** and **Figure 7**. Notice that the smaller coherent pairs has a little better shape coherence than the 1st shape coherent sets, however a bigger set, the 2nd one, has the best shape coherence factor of all.

Theory	$\alpha(A,B,T)$	Arc Length Change (%)	$\rho_\mu(A_t, A_{t+\tau})$	Specification
1st Shape coherent sets	0.9184	3.69 %	1	The grid size is 2000 by 200. See **Figure 6** left column.
2nd Shape coherent sets	0.9525	2.44 %	1	The grid size is 2000 by 200. See **Figure 7** left column.
Geodesic transport barrier	0.9156	1.2159 %	1	Calculated by LCStool [19]. See **Figure 6** right column.
Coherent pairs	0.9193	1.2174 %	0.992	80,000 by 80,000 matrix with 20 million sample points. See **Figure 7** right column.

slowly. On the other hand, according to the perspective of shape coherent sets, shape should be roughly preserved and the nonlinear flow restricted to that set should appear as a rigid body motion on that scale of time and space. This suggests that arc length may vary, however generally slowly. For coherent pairs, the definition [12] allows perfect overlap of a set and its image, so an extra condition called\robust must be added, which was later clarified in [11] [13] that effectively numerical diffusion was introduced in the stage of estimating the Ulam-Galerkin matrices that reward sets whose boundary curves do not grow dramatically. This suggests an implicit connection between the geodesic theory and the coherent pairs theory. See also [10]. **Table 2** and **Table 3** summarize a contrast study for benchmark examples, the Rossby wave and the double gyre system, where for the best possible comparison, a specific "coherent set" was found that seems to be roughly the same set as identified by all three perspectives. Therefore, the definition in each is not identical. Furthermore, there are numerical estimation issues that likely vary between each approach, as seen for example especially in the transfer operator method since many cells are required, and therefore many orbit samples for a reasonable estimate of a boundary curve.

It may seem striking that each method performs well on the measures of the other methods. There are of course differences between the methods as well, since each tends to identify sets that the other two do not, with significant difference in the non-corresponding measure. Note that we have used LCSTool [19] which uses closed shearlines, closed null-geodesics of the Green-Lagrange strain tensor, [18] which was pointed out to be

for incompressible flows; these are infinitesimally arc length conserving, but not generally. In the appendix, we show a simple example to demonstrate that there exist continuous families of different shapes with the same area and the same arc length.

2. Shape Coherence, Relative Coherence and Geodesic Transport Barrier

For completeness, in brief detail we review the three methods to be compared, with references to the originating literature for greater detail. Let $(\Omega, \mathcal{A}, \mu)$ be a measure space, where $\mathcal{A}$ is a σ-algebra and μ is a normalized measure that is not necessarily invariant. We assume that $\Omega \subset \mathbb{R}^2$. See [12] [21] [22]. Consider the planar nonautonomous differential equation [17],

$$\dot{x} = v(x,t), \quad x \in U \subset \mathbb{R}^2, t \in [t_-, t_+], \tag{1}$$

We use Φ to represent the flow map of the system[1].

2.1. Shape Coherence

Here we review shape coherence [22]. We recently introduced a definition concerning coherence called shape coherent sets[2], motivated by an intuitive idea of sets that "hold together" through finite-time. We connected shape coherent sets to slowly evolving boundary curvature by studying the tangency of finite-time stable and unstable foliations, which relate to forward and backward time perspectives respectively. The zero-angle curves are developed from the nonhyperbolic splitting of stable and unstable foliations by continuation methods that relate to the implicit function theorem. These closed zero-angle curves preserve their shapes in the time-dependent flow by a relatively small change of curvatures. See [22], on calculating the shape coherence factor. Taking a Lagrangian perspective, we offer the following mathematical definition:

Definition 1 [22] **Finite Time Shape Coherence** *The shape coherence factor* α *between two measurable nonempty sets* A *and* B *under a flow* Φ_t *after a finite time epoch* $t \in 0 : T$ *is,*

$$\alpha(A,B,T) := \sup_{S(B)} \frac{m(S(B) \cap \Phi_T(A))}{m(B)} \tag{2}$$

where $S(B)$ is a group of transformations of rigid body motions of B, specifically translations and rotations descriptive of *frame invariance,* and for certain problems it may include mirror translations. We interpret $m(\cdot)$ to denote Lebesgue measure, but one may substitute other measures as desired. Then we say A is finite time shape coherent to B with the factor α under the flow Φ_T after the time epoch T, but we may say simply that A is shape coherent to B. We shall call B the *reference set*, and A shall be called the *dynamic set*. In other words, if the flow Φ_T is restricted to a shape coherent set A, then $\Phi_T|_A$ can be considered to be approximately equivalent to a transformation which belongs to the group S, rigid body transformations. Throughout this paper we choose B to be A itself, which means we try to capture those sets with minimal shape change under the flow. Next, we introduce the finite-time stable and unstable foliations which are used to develop the boundaries of the shape coherent sets.

Stated simply, the stable foliation at a point describes the dominant direction of local contraction in forward time, and the unstable foliation describes the dominant direction of contraction in "backward" time. See **Figure 1** and **Figure 2**. They are also called Lyapunov vectors. Generally, the Jacobian matrix, $D\Phi_t(z)$ of the flow $\Phi_t(\cdot)$ evaluated at the point z has the same action as does any matrix in that a circle maps onto an ellipse. In **Figure 1** and **Figure 2** we illustrate the general infinitesimal geometry of a small disc of variations εw from a base point $\Phi_t(z)$. At z, we observe that a circle of such vectors, $w = <\cos(\theta), \sin(\theta)>, 0 \le \theta \le 2\pi$ centered at the point $\Phi_t(z)$ pulls back under $D\Phi_{-t}(\Phi_t(z))$ to an ellipsoid centered on z. The major axis of that infinitesimal ellipsoid defines $f_s^t(z)$, the stable foliation at z. Likewise, from $\Phi_{-t}(z)$, a small disc of variations pushes forward under $D\Phi_t(\Phi_{-t}(z))$ to an ellipsoid, again centered on z. The major axis of this ellipsoid defines the unstable foliations, $f_u^t(z)$.

To compute the major axis of ellipsoids corresponding to how discs evolve under the action of matrices, we

---

[1]The form of Φ may vary, such as $\Phi_{t_0}^t$, Φ_T and $\Phi(z,t;\tau)$, because we keep the original forms from different theories for better understanding. However, they represent the same flow.

[2]In this paper, we always use the initial status of a closed curve as its reference sets, *i.e.* as B in Equation (2).
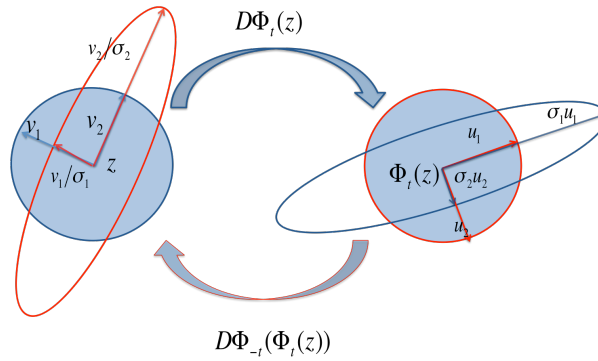
Figure 1. The SVD Equation (3) of the flow $\Phi_t(z)$ can be used to infer the finite time stable foliation and likewise finite time unstable foliation $f_u^t(z)$ at z in terms of the major and minor axis as shown and described in Equation (4).
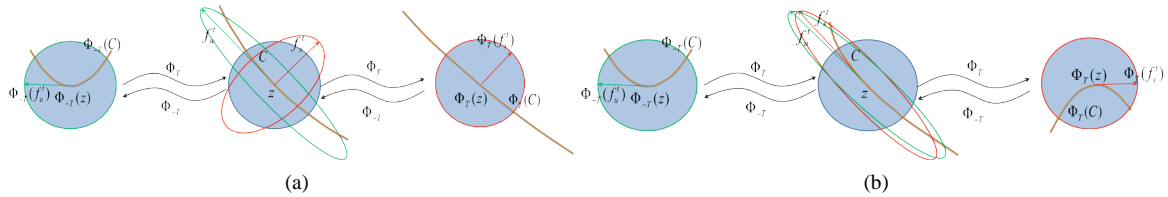

(a)   (b)

Figure 2. (a) A curve C goes through a small neighborhood of a point z with 90 degree foliations angle changes its shape from time $-T$ to T. Notice that the curve changes its curvature significantly in time, and it can increase or decrease curvature depending on the details of how the curve is oriented relative to $f_s^t(z)$ and $f_u^t(z)$; (b) The same curve C but with *almost* zero-splitting foliations roughly keeps its shape as noted by inspecting the curvature at z through time.

may refer to the singular value decomposition [14]. Let,

$$D\Phi_t(z) = U\Sigma V^*, \tag{3}$$

where $*$ denotes the transpose of a matrix, U and V are orthogonal matrices, and $\Sigma = diag(\sigma_1, \sigma_2)$ is a diagonal matrix. By convention we choose the index to order, $\sigma_1 \geq \sigma_2 \geq 0$. As part of the standard singular value decomposition theory, principal component analysis provides that the first unit column vector of $V = [v_1 \,|\, v_2]$ corresponding to the largest singular value, σ_1, is the major axis of the image of a circle under the matrix $D\Phi_t(z)$ around z. That is, $D\Phi_t(z)v_1 = \sigma_1 u_1$, as seen in **Figure 1** describes the vector v_1 at z that maps onto the major axis, σu_1 at $\Phi_t(z)$. Since $\Phi_{-t} \circ \Phi_t(z) = z$, and $D\Phi_{-t}(\Phi_t(z))D\Phi_t(z) = I$, then recalling the orthogonality of U and V, it can be shown that, $D\Phi_{-t}(\Phi_t(z)) = V\Sigma^{-1}U^*$, and $\Sigma^{-1} = diag(1/\sigma_1, 1/\sigma_2)$. Therefore, $1/\sigma_2 \geq 1/\sigma_1$, and the dominant axis of the image of an infinitesimal circle from $\Phi_t(z)$ comes from, $D\Phi_t(z)u_2 = v_2/\sigma_2$.

We summarize, the stable foliation and unstable foliation at z are,

$$f_s^t(z) = v_2 \ and \ f_u^t(z) = \overline{u}_1 \tag{4}$$

where v_2 is the second right singular vector of $D\Phi_t(z)$, according to Equation (3). And $\overline{u}_1$ is the first left singular vector of the matrix decomposition, $D\Phi_t(\Phi_{-t}(z)) = \overline{U} \ \overline{\Sigma} \ \overline{V}^*$. An included angle between a pair of stable and unstable foliations is defined as follows,

Definition 2 [22] *The included angle of the finite-time stable and unstable foliations is defined as* $\theta(z,t) : \Omega \times R^+ \to [-\pi/2, \pi/2]$

$$\theta(z,t) := \arccos \frac{\left\langle f_s^t(z), f_u^t(z) \right\rangle}{\left\| f_s^t(z) \right\| \left\| f_u^t(z) \right\|} \tag{5}$$

We give a comprehensive discussion of how the non-hyperbolic splitting angle of foliations preserves curvature of a curve in [22], and in turn, slowly changing of curvature yields significant shape coherence as noticed above. In order to generate curves of the zero-splitting angle, we apply the implicit function theorem to induce a continuation theorem, which guarantees that we can use ODE solvers and root-finding methods to describe the curve.

To calculate the shape coherence number is a form of "image registration", which is the process of transforming different image data into one coordinate system. See [1]-[4]. Image registration is a widely used class of algorithms in the image processing community to solve the following practical problem. Suppose two images (photographs for example) have pieces of the same scene such as a car or a face, then how can the two images be best "aligned" so as to place one figure on top of the other in a manner that emphasizes that the scenes are aligned. By aligned we mean that rotations, and translations may be used, and in the image processing problem often linear scalings as well, but we will not use that class of transformation. In other words, alignment in terms of rigid body motions of two sets is equivalent to the image processing problem of registration, and it is a convenient comparison since image registration is a well matured problem with many fast and accurate algorithms, including methods based on Fourier Transforms, [1] [4]. Since we assume the flow is area-preserving, generally, we use rigid body motions and may include mirror. In Matlab, the command "imregister" is a convenient implementation of image registration. For more details on the algorithm, see [22].

2.2. The Geodesic Theory of LCS

Next, we review the geodesic theory of Lagrangian coherent structures. Consider an evolving material line γ_t in the system, which has length

$$l(\gamma_t) = \int_{\gamma_t} | dx | = \int_a^b | D\Phi_{t_0}^t(r)dr | = \int_{s_1}^{s_2} \sqrt{\langle r', C_{t_0}^t(r)r' \rangle} ds \tag{6}$$

where $D\Phi_{t_0}^t(x_0)$ denotes the derivative of the flow map, and $C_{t_0}^t = (D\Phi_{t_0}^t(x_0))^T D\Phi_{t_0}^t(x_0)$ denotes the Cauchy-Green strain tensor, with T refering to the matrix transpose. In [17], a **transport barrier** of system 1 over the time interval $[t_0, t]$ was described as a material curve γ_t, whose initial position γ_0 is a minimizer of the length functional $l_{t_0}^t$ under the boundary conditions,

$$r(s_2) \neq r(s_1), \quad r'(s_i) = \xi_1(r(s_i)), \quad i = 1, 2 \tag{7}$$

$$h(s_{1,2}) = 0, \ r'(s_1) = \eta_{\pm}(r(s_1)), \ r'(s_2) = \eta_{\pm}(r(s_2)), \ r(s_1) \neq r(s_2), \tag{8}$$

where $\xi_{1,2}$ are the eigenvectors corresponding to the smaller and larger eigenvalues $\lambda_{1,2}(r(s_{1,2}))$ of $C_{t_0}^t(r(s_{1,2}))$, $h(s_{1,2})$ is a pointwise normal, smooth perturbation to γ_0 and $\eta_{\pm}(x)$ are the normalized Lagrangian shear vector fields, which are defined as, $\eta_{\pm} = \sqrt{\frac{\sqrt{\lambda_2}}{\sqrt{\lambda_1} + \sqrt{\lambda_2}}} \xi_1 \pm \sqrt{\frac{\sqrt{\lambda_1}}{\sqrt{\lambda_1} + \sqrt{\lambda_2}}} \xi_2$. A transport barrier is a **hyperbolic barrier** if γ_0 satisfies the hyperbolic boundary conditions as defined in Equation (7). A transport barrier is a **shear barrier** if γ_0 satisfies the shear boundary conditions as defined in Equation (8). For the computational part, for comparison here we use the the "LCS-tools" which were developed by the Nonlinear Dynamical Systems Group at ETH Zurich, led by Prof. George Haller. See. [19].

2.3. The Relatively Coherent Pairs

In this section, we briefly review the coherent pairs. Relatively coherent pairs [21] describe a system by hierarchical partitions based on the idea of coherent pairs. See [12]. Given the time-dependent flow $\Phi(z, t; \tau) : \Omega \times \mathbb{R} \times \mathbb{R} \to \Omega$, through the time epoch τ of an initial point z at time t, a coherent pairs $(A_t, A_{t+\tau})$ can be considered as a pair of subsets of Ω such that, $\Phi(A_t, t; \tau) \approx A_{t+\tau}$.

Definition 3 [12] $(A_t, A_{t+\tau})$ *is a* (ρ_0, t, τ) *-coherent pair if*

$$\rho_\mu(A_t, A_{t+\tau}) := \mu(A_t \cap \Phi(A_{t+\tau}, t+\tau, -\tau)) / \mu(A_t) \geq \rho_0 \tag{9}$$

where the pair $(A_t, A_{t+\tau})$ are 'robust' to small perturbation and $\mu(A_t) = \mu(A_{t+\tau})$.

Then we build a relative measure on K induced by μ, where K is a nonempty measurable subset of Ω. In this way we enter into refinements of the initial partition on successive scales. A **relative measure** of K to

Ω is, [21], $\mu_K(A) := \mu(A \cap K) / \mu(K)$ for all $A \in \mathcal{A}$. From the above definition, it follows that $(K, \mathcal{A}|_K, \mu_K)$ is also a measure space, where $\mathcal{A}|_K$ is the restriction of Ω to $\mathcal{A}$ and μ_K is a normalized measure on K. We call the space $(K, \mathcal{A}|_K, \mu_K)$, the *relative measure space*. Now, we define the *relatively coherent pairs*.

Definition 4 [21] *Relatively coherent structures are those* (ρ_0, t, τ)*-coherent pairs defined in Definition* 2.1, *with respect to given relative measures on a subset* $K \subset \Omega$, *of a given scale, specializing* [12].

To find coherent pairs in time-dependent dynamical systems, we use the Frobenius-Perron operator. If $S : \Omega \to \Omega$ is a nonsingular transformation such that $\mu(S^{-1}(A)) = 0$ for all $A \in \mathcal{A}$ satisfying $\mu(A) = 0$, the unique operator $P : L^1(\Omega) \to L^1(\Omega)$ defined by,

$$\int_A Pf(x)\mu(dx) = \int_{S^{-1}(A)} f(x)\mu(dx) \tag{10}$$

for all $A \in \mathcal{A}$ is called the Frobenius-Perron operator corresponding to S, where $f(x) \in L^1(\Omega)$. See [2] [20]. Here, S can be considered as the flow map Φ and the formula above can be written as $P_{t,\tau}f(z) := f(S^{-1}(z)) \cdot |\det D(S^{-1}(z))| = f(\Phi(z, t+\tau; -\tau)) \cdot |\det D\Phi(z, t+\tau; -\tau)|$. Suppose X is a subset of Ω, and let Y be a set that includes $S(X)$. We develop partitions for X and Y respectively. In other words, let $\{B_i\}_{i=1}^m$ be a partition for X and $\{C_j\}_{j=1}^n$ be a partition for Y. The Ulam-Galerkin matrix follows a well-known finite-rank approximation of the Frobenius-Perron operator,

$$P_{i,j} = \#\{x_k : x_k \in B_i \ \& \ S(x_k) \in C_j\} / \#\{x_k : x_k \in B_i\}$$

where the sequence $\{x_k\}$ is a set of test points (passive tracers). See [5]. The computation of coherent pairs is a set-oriented method, but to compare the results to the other two methods which are defined in terms of boundary curves of sets, we must extract boundary curves from the boundaries that are approximated by the set of triangles covering the boundary, [21]. An effective way to extract the boundary is to shrink the size of triangles; then we approximate the boundary by connecting the centers of triangles on these boundary sets, and this is done either by line segments through adjacent triangles, or it could be done with some smoothing by a pair of smoothing splines.

3. Examples

We next apply the three methods to the Rossby wave system and double gyre system, both of which have become classic examples for studying and contrasting coherence and transport, [2] [10] [12] [17] [21].

3.1. The Nonautonomous Double Gyre.

Consider the nonautonomous double gyre system,

$$\dot{x} = -\pi A \sin(\pi f(x,t))\cos(\pi y) \ and \ \dot{y} = \pi A \cos(\pi f(x,t))\sin(\pi y)\frac{df}{dx} \tag{11}$$

where $f(x,t) = \varepsilon \sin(\omega t)x^2 + (1 - 2\varepsilon \sin(\omega t))x$, $\varepsilon = 0.1$, $A = 0.1$ and $\omega = 2\pi/10$. See [10] [25]. Let the time interval be $[0, 20]$. **Table 2**, **Figure 3** and **Figure 4** show the numerical results of the comparison among the three theories of the nonautonomous double gyre system.

Consider the example sets shown. Note that the LCS has the smallest arc length change, but the shape coherent sets have the highest shape coherence factor. While the coherent pair number of both the shape coherence derived set and the geodesic transport derived set are shown as 1, since if the image in definition Equation (9) is its image, as the pairing, then 1 will always be the result, but the theory is properly interpreted the entire definition of coherent pairs requires a more careful pairing of sets as discussed above. What is striking here is that three different methods can find comparable sets, as reflected that the measures are similar. On the other hand, not shown here, is that each can find different sets, but the measures between them would necessarily be dramatically different. See **Figure 4** for such a scenario where two methods sometimes produce substantially similar regions, but sometimes substantially different regions.

3.2. An Idealized Stratospheric Flow

The second benchmark problem is a quasiperiodic system which represents an idealized zonal stratospheric flow [12] [24]. Consider the following Hamiltonian system $dx/dt = -\partial\Phi/\partial y, dy/dt = \partial\Phi/\partial x$, where
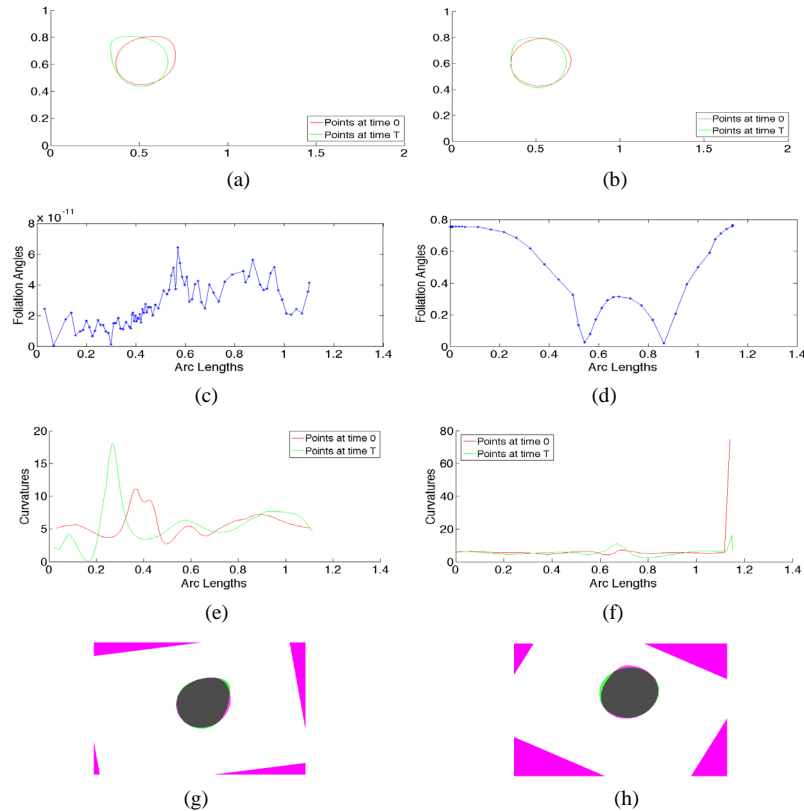
Figure 3. (a) and (b) show the initial and final configuration of a zero-splitting curve (Left) and an elliptic LCS (Right) around the zero-splitting curve. (c) and (d) are the comparison of foliation angles versus arc lengths between the two curves. The foliation angles of the zero-splitting curves are very small, but the angles of the geodesic curve vary. (e) and (f) are the curvature versus arc lengths. (g) and (h) are registrations of the curves. The arc lengths change of the zero-splitting curve and the elliptic LCS are 1.14% and 0.93%; and the shape coherence factors are 0.9637 and 0.9362. (a) A nonhyperbolic splitting curve; (b)An elliptic LCS; (c) Foliations angles of the nonhyperbolic splitting curve; (d) Foliations angles of the elliptic LCS; (e) Curvature change of the nonhyperbolic splitting curve; (f) Curvature change of the elliptic LCS.
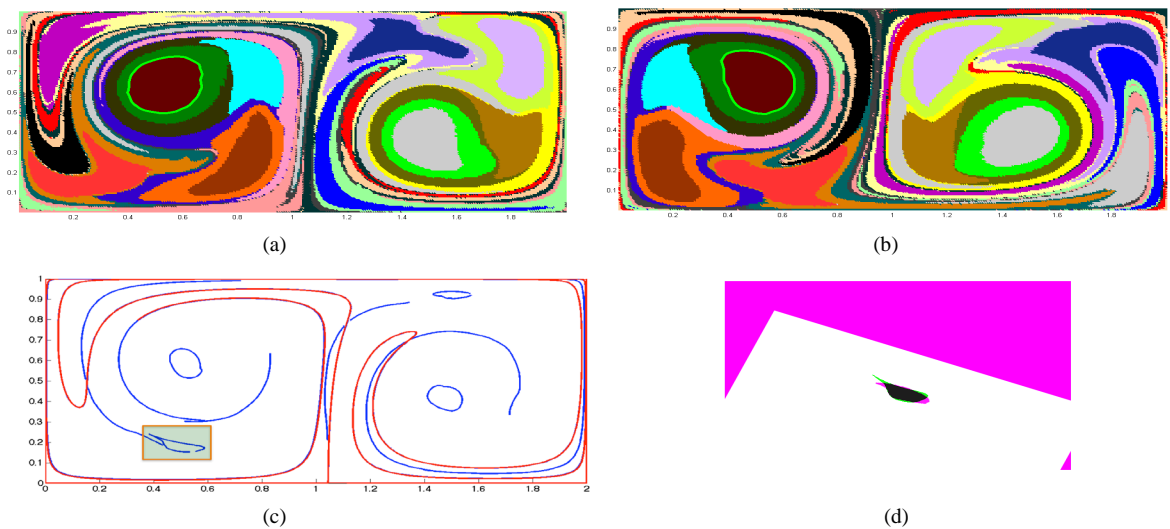

Figure 4. (a) and (b) are the hierarchical partitions of the double gyre. The green curves around the upper left brown sets are the boundaries of our target coherent pairs. (c) and (d) are the foliation angles and change of curvature plot in different time. The arc lengths change is 1.9% and the shape coherence factor is 0.9210. (a) Relatively coherent sets at $T = 0$; (b) Relatively coherent sets at $T = 20$; (c) Foliations angles of the coherent pairs; (d) Curvature change of the coherent pairs.

$$\Phi(x, y, t) = c_3 y - U_0 L \tanh(y/L) + A_3 U_0 L sech^2(y/L) \cos(k_1 x)$$
$$+ A_2 U_0 L sech^2(y/L) \cos(k_2 x - \sigma_2 t) + A_1 U_0 L sech^2(y/L) \cos(k_1 x - \sigma_1 t)$$

(12)

Let $U_0 = 41.31, c_2 = 0.205 U_0, c_3 = 0.461 U_0, A_3 = 0.3, A_2 = 0.1, A_1 = 0.075$ and the other parameters be the same as stated in [24]. The numerical results in **Table 3**, **Figure 5** and **Figure 6** show that the elliptic LCS shown maintains arc length better than the other three curves also in this system, but the coherent pairs have a shape coherence factor a little greater than the first smaller shape coherent sets. Note that although these measurements are so close, that it could be inferred that differences are within the level of numerical accuracy. The degree of coherence becomes rarer for bigger regions, than smaller ones, so we show the second shape coherent sets as a bigger one with the highest shape coherence factor. See **Table 3**. Again we see each does especially well within its own measures, but quite well across measures. So while each method can and often does develop comparable sets, sometimes they develop dramatically different sets. See **Figure 4**. It is shown there that the two perspectives often do reveal extremely similar boundaries, but sometimes quite different ones.

4. Conclusions

In this paper, we have reviewed three complementary theories of coherence that come with similar goals but from different perspectives. These are the geodesic theory of LCS which emphasizes stationarity of averaged strain and shear, coherent pairs which describes "very small leakage" of sets and shape coherent sets which emphasizes those sets that preserve their shape by a slowly evolving curvature.

We have then presented two benchmark examples, the double gyre and the Rossby wave, to compare the different methods. In the examples described here, it has been illustrated that all three methods have reasonable and similar numerical results which agree with their own theories, and comparable results between given that similar sets were identified. For arc length, LCS always has the least change; and with respect to shape coherence, the zero-splitting curve has the best shape coherence number; coherent pairs has results very close to them. Notice that here we only compared similar elliptic shapes for all three methods, to allow each the best possibility of doing well relative to each other. On the other hand, each of the three methods can and does find clearly different sets and therefore with significant differences of performance measure. See **Figure 7**.
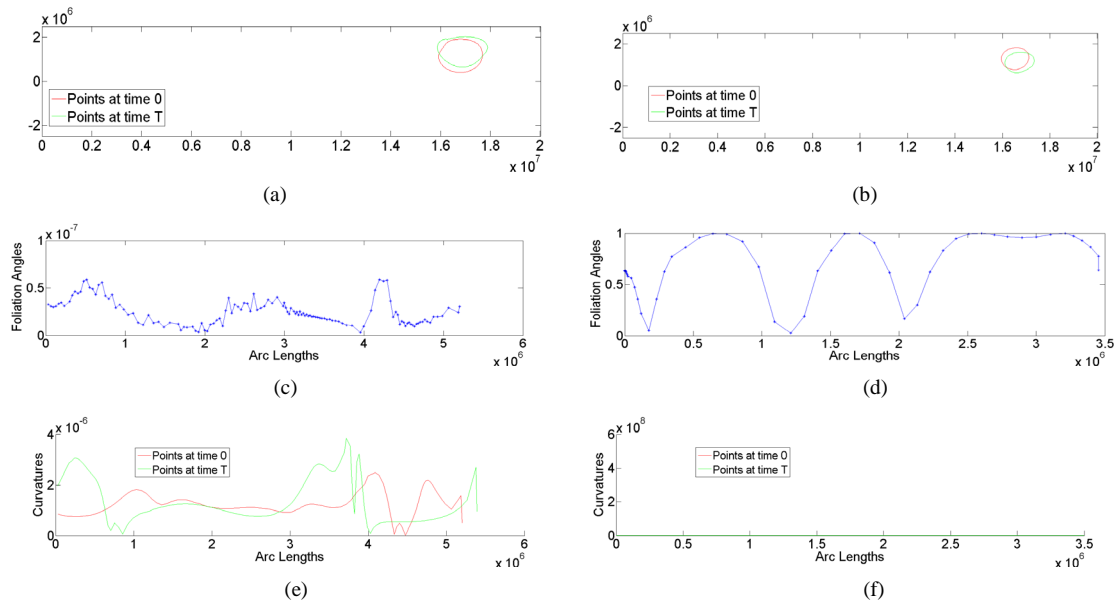

Figure 5. (c) shows that the angle of zero-splitting curve keep small. From (e) and (f) we can see that the zero-splitting curve has the less change of curvature. The zero-splitting curve is the closest one to the elliptic LCS, but there are still differences on size. **Figure 6** shows a bigger zero-splitting curve. The arc lengths change of the zero-splitting curve and the elliptic LCS are 3.69% and 1.2159%; and the shape coherence factors are 0.9184 and 0.9156. (a) A nonhyperbolic splitting curve; (b) An elliptic LCS; (c) Foliations angles of the nonhyperbolic splitting curve; (d) Foliations angles of the elliptic LCS; (e) Curvature change of the nonhyperbolic splitting curve; (f) Curvature change of the elliptic LCS.
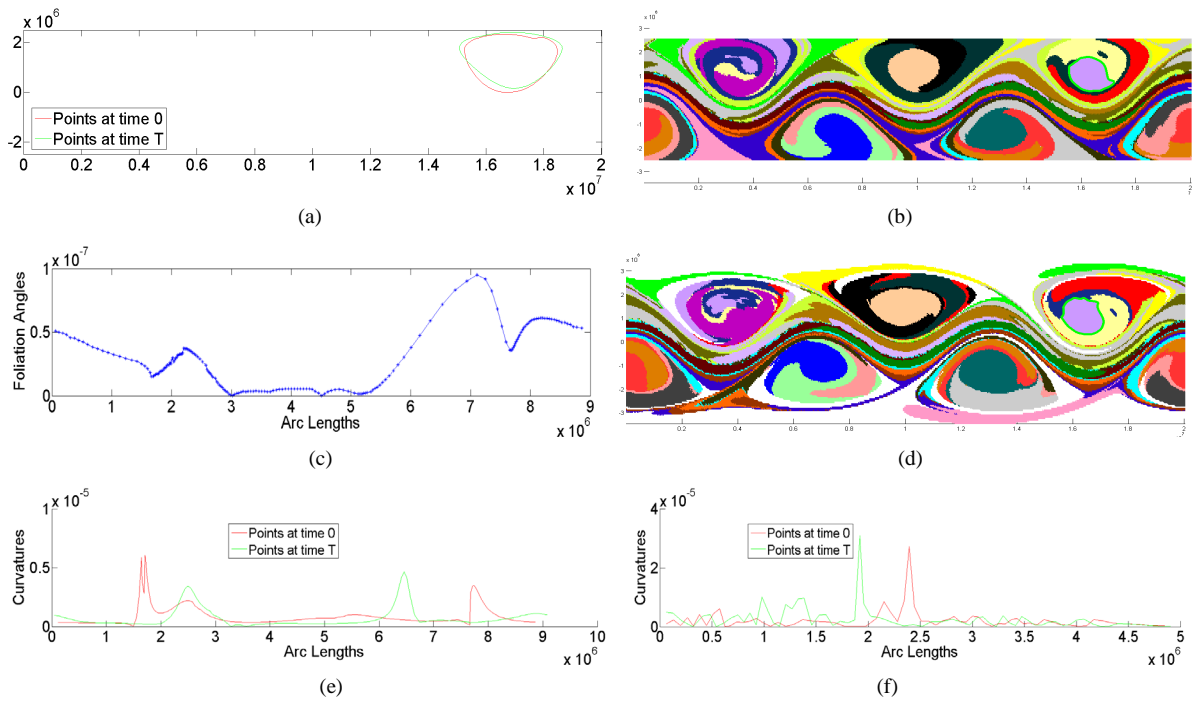
Figure 6. We observe that the zero-splitting curve keep better curvature than the coherent pairs, though the shape of zero-splitting curve is bigger. The arc lengths change of the zero-splitting curve and the coherent pairs are 2.44% and 1.2174%; and the shape coherence factors are 0.9525 and 0.9193. (a) A nonhyperbolic splitting curve; (b) Initial status of the coherent pairs; (c) Foliations angles of the nonhyperbolic splitting curve; (d) Final status of the coherent pairs; (e) Curvature change of the nonhyperbolic splitting curve; (f) Curvature change of the coherent pairs.
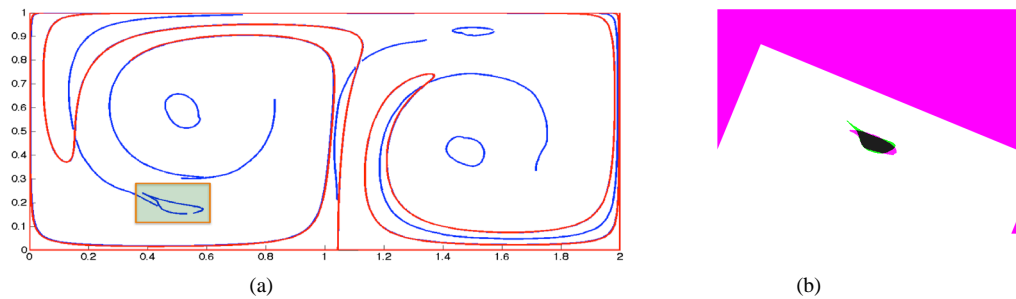

Figure 7. Contrasting regions described by LCS and Shape Coherence. (a) LCS curves shown in red are contrasted to curves of slowly changing curvature in blue, which are meant to lead to shape coherent sets when they are closed. We see here that often the two perspectives lead to similar sets since the blue and red curves are extremely close to each other, but sometimes they are not close at all. Extracting one such set shows that the slowly changing curvature sets are significantly shape coherent when considered in terms of image registration (optimal rigid body transformations); (b) A set of slowly changing curvature (blue) highlighted by a box above is extracted and then evolved as shown here under optimal registration demonstrating its degree of shape coherence.

We have not found an a priori reason to expect that each of the three definitions of coherence will usually, or even often, find the same sets. A theorem directly connecting them is lacking. Indeed sometimes we find that each finds sets that the others do not, but in such a case, a numerical comparison of the measures included here only points out dramatic differences. Stated in terms of choice, a practitioner may ask which method to use for their own applied problem, but there is no magic bullet or best method to compute coherence. By offering the contrasting perspective of three different concepts of the general idea of coherence, in the same light, we hope that this discussion offers the practitioner a richer mathematical perspective of what is the outcome of what they are computing, no matter what method they choose to use.

References

[1] Brown, L.G. (1992) A Survey of Image Registration Techniques. *ACM Computing Surveys* (*CSUR*), **24**, 325-376. http://dx.doi.org/10.1145/146370.146374

[2] Bollt, E. and Santitissadeekorn, N. (2013) Applied and Computational Measurable Dynamics. SIAM. http://dx.doi.org/10.1137/1.9781611972641

[3] Barnea, D.I. and Silverman, H.F. (1972) A Class of Algorithms for Fast Digital Registration. *IEEE Trans. Comput.*, **C-21**, 179-186. http://dx.doi.org/10.1109/TC.1972.5008923

[4] De Castro, E. and Morandi, C. (1987) Registration of Translated and Rotated Images Using Finite Fourier Transforms. *IEEE Thans. Pattern Anal. Machine Intell.*, **PAMI-95**, 700-703. http://dx.doi.org/10.1109/TPAMI.1987.4767966

[5] Ding, J., Li, T.Y. and Zhou, A. (2002) Finite Approximations of Markov Operators. *Journal of Computational and Applied Mathematics*, **147-1**, 137-152. http://dx.doi.org/10.1016/s0377-0427(02)00429-6

[6] Froyland, G. (2005) Statistically Optimal Almost-Invariant Sets. *Physica D*: *Nonlinear Phenomena*, **200**, 205-219. http://dx.doi.org/10.1016/j.physd.2004.11.008

[7] Farazmand, M. and Haller, G. (2012) Computing Lagrangian Coherent Structures from Their Variational Theory. *Chaos*, **22**, 013128. http://dx.doi.org/10.1063/1.3690153

[8] Farazmand, M. and Haller, G. (2013) Attracting and Repelling Lagrangian Coherent Structures from a Single Computation. *Chaos*, **23**, 023101. http://dx.doi.org/10.1063/1.4800210

[9] Farazmand, M. and Haller, G. (2012) Erratum and Addendum to "A Variational Theory of Hyperbolic Lagrangian Coherent Structures" [Physica D 240 (2011) 574–598]. *Physica D*, **241** 439-441. http://dx.doi.org/10.1016/j.physd.2011.09.013

[10] Froyland, G. and Padberg, K. (2009) Almost-Invariant Sets and Invariant Manifolds-Connecting Probabilistic and Geometric Descriptions of Coherent Structures in Flows. *Physica D*, **238**, 1507-1523. http://dx.doi.org/10.1016/j.physd.2009.03.002

[11] Froyland, G. and Padberg, K. (2014) Almost-Invariant and Finite-Time Coherent Sets: Directionality, Duration, and Diffusion. To appear in *Ergodic Theory*, *Open Dynamics*, *and Coherent Structures*, **70**, 171-216. http://dx.doi.org/10.1007/978-1-4939-0419-8_9

[12] Froyland, G., Santitissadeekorn, N. and Monahan, A. (2010) Transport in Time-Dependent Dynamical Systems: Finite-Time Coherent Sets. *Chaos*, **20**, 043116. http://dx.doi.org/10.1063/1.3502450

[13] Froyland, G. (2013) An Analytic Framework for Identifying Finite-Time Coherent Sets in Time-Dependent Dynamical Systems. *Physica D*, **250**, 1-19. http://dx.doi.org/10.1016/j.physd.2013.01.013

[14] Golub, G.H. and Van Loan, C.F. (1989) Matrix Computations. 2nd Edition, The Johns Hopkins University Press.

[15] Haller, G. (2000) Finding Finite-Time Invariant Manifolds in Two-Dimensional Velocity Fields. *Chaos*, **10**, 99. http://dx.doi.org/10.1063/1.166479

[16] Haller, G. (2002) Lagrangian Coherent Structures from Approximate Velocity Data. *Physics of Fluids*, **14**, 1851. http://dx.doi.org/10.1063/1.1477449

[17] Haller, G. and Beron-Vera, F.J. (2012) Geodesic Theory of Transport Barriers in Two-Dimensional Flows. *Physica D*, **241**, 1680-1702. http://dx.doi.org/10.1016/j.physd.2012.06.012

[18] Haller, G. and Beron-Vera, F.J. (2013) Coherent Lagrangian Vortices: The Black Holes of Turbulence. *J. Fluid Mech.* **731**. http://dx.doi.org/10.1017/jfm.2013.391

[19] NDSG at ETH Zurich, Led by Prof. Haller, G., *LCS Tool*. https://github.com/jeixav/LCS-Tool

[20] Lasota, A. and Mackey, M.C. (1985) Chaos, Fractals, and Noise Stochastic Aspects of Dynamics. Springer.

[21] Ma, T. and Bollt, E. (2013) Relatively Coherent Sets as a Hierarchical Partition Method. *International Journal of Bifurcation and Chaos*, **23**, 1330026. http://dx.doi.org/10.1142/S0218127413300267

[22] Ma, T. and Bollt, E. (2014) Differential Geometry Perspective of Shape Coherence and Curvature Evolution by Finite-Time Nonhyperbolic Splitting. *SIADS*, **13**, 1106-1136. http://dx.doi.org/10.1137/130940633

[23] Ma, T. and Bollt, E. (2014) Shape Coherence and Finite-Time Curvature Evolution. To appear in *International Journal of Bifurcation and Chaos*, **25**.

[24] Rypina, I.I., Brown, M.G., Beron-Vera, F.J., Kocak, H., Olascoaga, M.J. and Udovydchenkov, I.A. (2007) On the Lagrangian Dynamics of Atmospheric Zonal Jets and the Permeability of the Stratospheric Polar Vortex. *Journal of the Atmospheric Sciences*, **64**.

[25] Shadden, S.C., Lekien, F. and Marsden, J.E. (2005) Definition and Properties of Lagrangian Coherent Structures from Finite-Time Lyapunov Exponents in Two-Dimensional Aperiodic Flows. *Physica D*, **212**, 271-304.

http://dx.doi.org/10.1016/j.physd.2005.10.007

[26] Tallapragada, P. and Ross, S.D. (2013) A Set Oriented Definition of Finite-Time Lyapunov Exponents and Coherent Sets. *Commun Nonlinear Sci Number Simulation*, **18**, 1106-1126. http://dx.doi.org/10.1016/j.cnsns.2012.09.017

Appendix

Here, we present an example of a continuous two-dimensional family of *simply connected sets with the same perimeter, and area, but different shapes*. By this observation, we argue that a closed geodesic transport barrier may lose its shape through the flow. **Figure 8** shows two simply connect sets, a rectangle A with height a and width a and an annulus sector B with angle θ, inner radius r and outer radius $r+h$. The perimeter and area of A are, P_A and S_A, $P_A = 2a + 2h$ *and* $S_A = ah$. And the perimeter and area of B are, P_B and S_B, $P_B = \dfrac{2\pi\theta(2r+h)}{360} + 2h$ *and* $S_B = \dfrac{\pi\theta(2rh + h^2)}{360}$. Now we assume the two shapes A and B have the same area and perimeter, so we have the relationships as follows,

$$P_A = P_B \quad and \quad S_A = S_B \Leftrightarrow a = \frac{\pi\theta(2r+h)}{360} \tag{13}$$

So, for example, let $h = 1$, $a = 10$, $r \approx 1.4$ and $\theta = 300\,\mathrm{deg}$, we have $P_A = P_B = 22$ and $S_A = S_B = 10$.
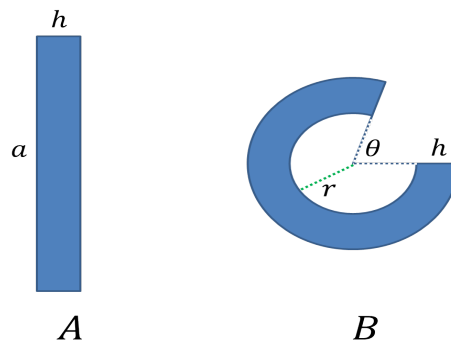

Figure 8. Two simply connected sets.